Available online at www.sciencedirect.com
SCIENCE DIRECT
Gondwana Research 9 (2006) 209 – 224
www.elsevier.com/locate/gr

Late Paleozoic retrograded eclogites from within the northern margin of the North China Craton: Evidence for subduction of the Paleo-Asian ocean

Zhiyao Ni [a,b,*], Mingguo Zhai [a], Renmin Wang [c], Ying Tong [d]

[a] Institute of Geology and Geophysics, Chinese Academy of Sciences, Beijing 100029, China
[b] College of Earth Sciences, Chengdu University of Technology, Chengdu, Sichuan 610059, China
[c] School of Earth and Space Sciences, Peking University, Beijing 100871, China
[d] Institute of Geology, Chinese Academy of Geological Sciences, Beijing 100037, China

Received 8 November 2004; accepted 25 June 2005

Abstract

Retrograded eclogites from the central part of the northern margin of the North China Craton, Hebei Province, China occur as separate tectonic lenses or boundins within garnet–biotite–plagioclase gneisses of the Paleoproterozoic Hongqiyingzi Complex characterized by amphibolite facies paragneisses. The petrographic features and mineralogical compositions represent three main metamorphic stages: (1) the peak eclogite facies stage ($P>1.40–1.50$ GPa, $T=680–730$ °C), (2) the granulite facies stage and (3) the amphibolite facies stage ($P=0.67–0.81$ GPa, $T=530–610$ °C) formed during decompression. The major and trace element and Sm–Nd isotopic data suggest that most of the retrograded eclogite samples had protoliths of tholeiitic oceanic crust with geochemical characteristics of mid-ocean ridge basalt (MORB) or island arc tholeiite (IAT) environment, and were contaminated by crustal components during subsequent subduction. Zircon SHRIMP isotopic dating of two different textural varieties of retrograded eclogite defines a weighted mean age of ~325 Ma, which is interpreted as the peak metamorphic age of the eclogites and reflects the occurrence of eclogite facies metamorphism related to subduction of Paleo-Asian Oceanic crust beneath the North China Craton during the Late Paleozoic. Finally, we show that the retrograded eclogite from Hebei Province is not related to the Baimashi retrograded eclogite at the northern foot of the Heng Mountains, approximately, 300 km to the southwest.
© 2006 International Association for Gondwana Research. Published by Elsevier B.V. All rights reserved.

Keywords: Retrograded eclogite; Paleo-Asian oceanic crust; Late Paleozoic; Hongqiyingzi Complex; North China Craton

1. Introduction

Eclogites are virtually absent from the North China Craton (NCC), the single example was reported from Baimashi, near the Heng Mountains (Hengshan), which are characterized by a vermicular symplectite of diopside and plagioclase, but no omphacite (Zhai et al., 1996; Zhao et al., 2001). Therefore the new discovery of retrograded eclogites reported in this study is important with regard to understanding the tectonic evolution of the NCC.

This paper presents new petrological, geochemical and geochronological data on recently discovered retrograded eclogites from the central part of the northern margin of the NCC. We also discuss (1) the protolith of the retrograded eclogite, (2) the timing of peak eclogite facies metamorphism, and (3) the importance of retrograded eclogite and its tectonic implications.

2. Regional geology

The North China Craton (NCC) refers to the Chinese part of the Sino-Korea Craton. It is surrounded by younger Phanerozoic orogenic belts (Fig. 1a). The Late Paleozoic Tianshan–Inner Mongolia–Daxinganling Orogenic Belt (also known as the Paleo-Asian Ocean tectonic region or the Central Asian Orogenic Belt) bounds the craton to the north. Traditionally, it was considered that the NCC was cratonized at ca. 2500 Ma and is mainly composed of granulite to upper amphibolite facies metamorphic rocks and granitoids (Zhai, 1996). Recently, however, two different models have been proposed for the tectonic framework of the NCC based on lithological,

* Corresponding author. Institute of Geology and Geophysics, Chinese Academy of Sciences, Beijing 100029, China.
E-mail address: nizyao@cdut.edu.cn (Z. Ni).

1342-937X/$ - see front matter © 2006 International Association for Gondwana Research. Published by Elsevier B.V. All rights reserved.
doi:10.1016/j.gr.2005.06.014

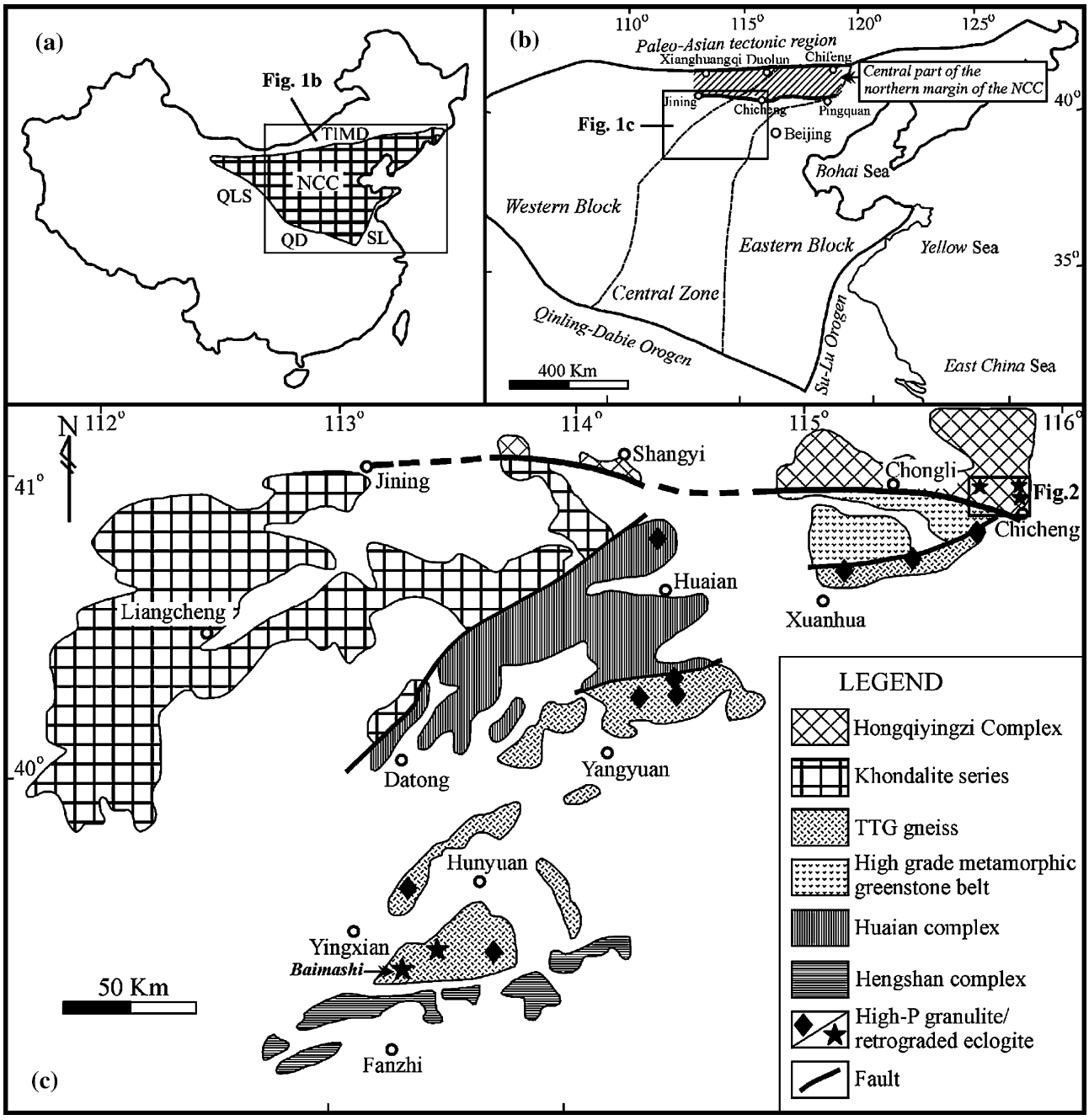

Fig. 1. (a) Location of the North China Craton (NCC) showing the major Phanerozoic orogenic belts. TIMD: Tianshan–Inner Mongolia–Daxinganling Orogen; QLS: Qilianshan Orogen; QD: Qinlin–Dabie Orogen; SL: Su–Lu Orogen. (b) Tectonic framework of the NCC, showing the tectonic setting of the central part of the northern margin of the NCC (modified from Guo et al., 2005). (c) Geological sketch map showing distribution of the retrograded eclogites in the NCC (modified from Guo et al., 1996, 2005).

structural, metamorphic and geochronological data. The first model subdivided the NCC into Western and Eastern Blocks separated by a Central zone (Fig. 1b) interpreted as a Paleoproterozoic (ca. 1.85–1.80 Ga) continental collision orogenic zone between the other two blocks (Zhao et al., 1998, 1999, 2000; Zhao, 2001). The second model also distinguished a collision zone between the Western and Eastern Blocks although the extent of the above blocks differs from the first model and, more importantly, the time of the collision is earlier assumed as ca. 2.5 Ga has been revised as Paleoproterozoic (ca. 1.85–1.80 Ga) within continental rift setting (Zhai et al., 2000; Li et al., 2000; Kusky and Li, 2003).

The central part of the northern margin of the NCC is bounded by the Xianghuangqi–Duolun–Chifeng fault belt (XDCB) to the north. To the south, this region is bounded by the Jining–Chicheng–Pingquan fault belt (JCPB) (Fig. 1b, c). The major stratigraphic unit within the central part of the northern margin of the NCC is the Paleoproterozoic Hongqiyingzi Complex which is extensively developed and contains many ultramafic rock enclaves. It is composed of

amphibolite facies volcano-sedimentary rocks, including garnet- or amphibole-bearing biotite–plagioclase gneisses, biotite–plagioclase amphibolites and minor magnetite quartzites and calcareous or muddy marbles, with published ages ranging from 2000–2450 Ma (Hu et al., 1996). These lithologic units have an E–W trending foliation and distinct remnant bedding.

The retrograded eclogites, which were previously incorrectly described as high-pressure garnet amphibolites (Qian et al., 1996), occur as separate tectonic lenses or boundins within biotite–plagioclase gneisses of the Paleoproterozoic Hongqiyingzi Complex, which consist of biotite, plagioclase, quartz and minor garnet or amphibole. The retrograded eclogites are exposed at Zhenningbu, Luhebu and Qilidun villages near the JCPB and Chicheng Town (Fig. 2). Retrograded eclogite boundins or lenses vary from 4–5 cm to 40–50 m in size, and are most abundant at Luhebu village (Fig. 3). Their elongation is consistent with the regional schistosity of the biotite–plagioclase gneisses.

3. Petrography and mineral chemistry

The mineral compositions were analyzed using a JEOL JXA 8100 electron microprobe at the School of Earth and Space Sciences, Peking University. The operating conditions were 15 kV accelerating voltage, 10 nA beam current, and 1 μm beam diameter. Minerals from the Standard 02753-AB of American SPI Company was used as standards for all elements. The results are presented in Tables 1 and 2.

Based on the degree of amphibolitization, the retrograded eclogites can be divided into two types. One is weakly amphibolitized retrograded eclogite, identified as omphacite-bearing garnet granulite, and the other is intensely amphibolitized retrograded eclogite, that includes garnet amphibolite, garnet–plagioclase amphibolite and minor plagioclase amphibolite.

The weakly amphibolitized eclogite was collected from Luhebu village (Fig. 3). It mainly consists of garnet and a vermicular symplectite of clinopyroxene-plagioclase (Fig. 4a).

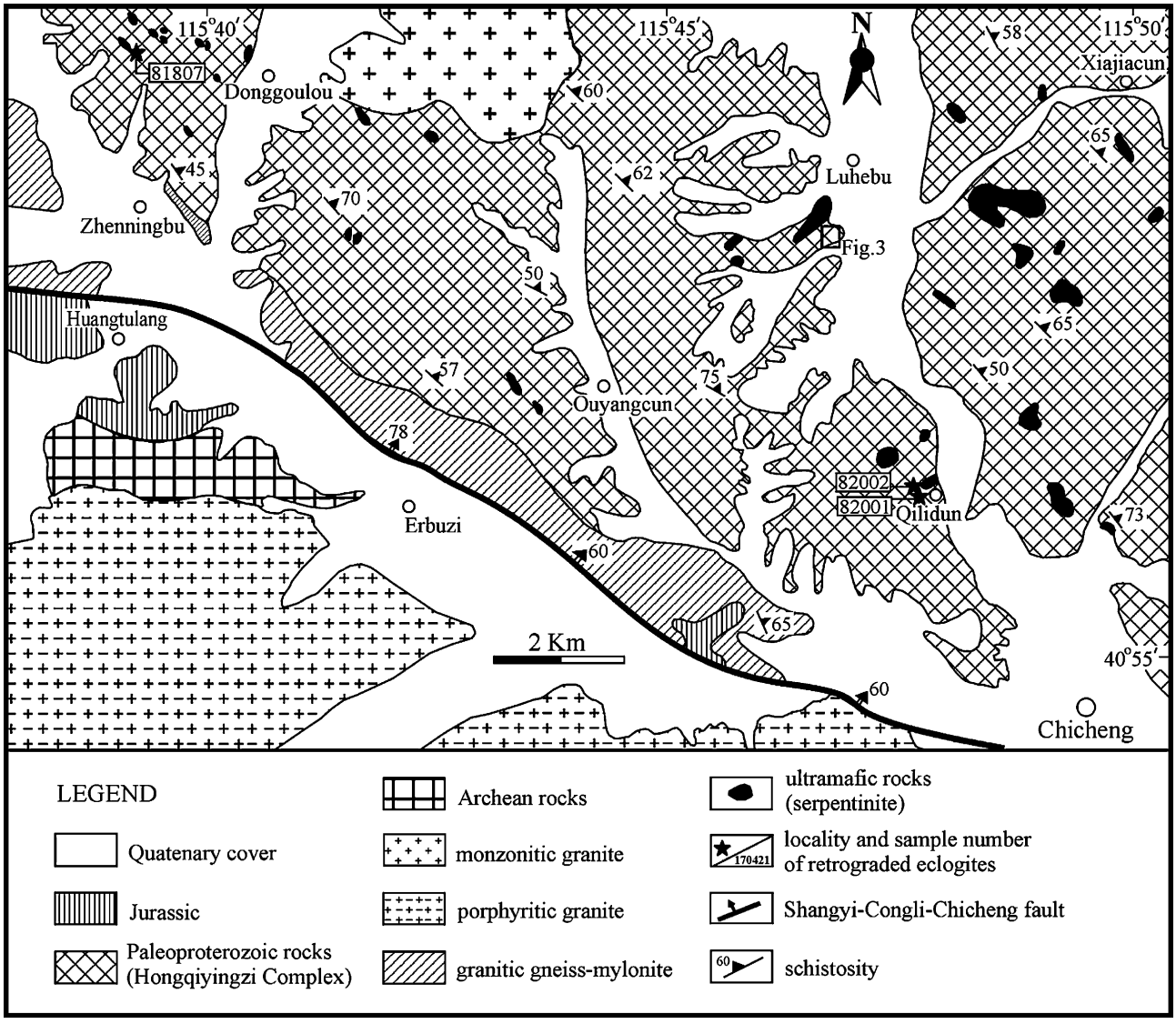

Fig. 2. Geological map showing locations of retrogressed eclogite from Chicheng.

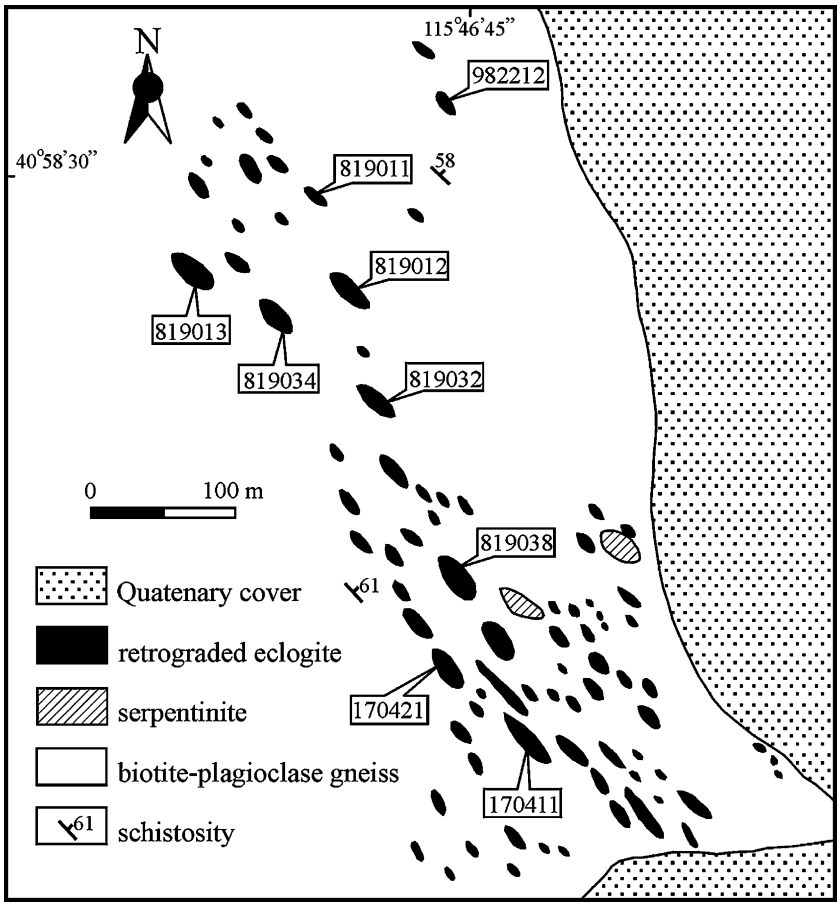

Fig. 3. A close up geological map showing location of retrogressed eclogite near Luhebu village.

Some of these rocks have been partially altered to amphibolite facies paragneisses by the replacement of vermicular symplectitic clinopyroxene by amphibole and by the development of narrow amphibole–plagioclase kelyphitic rim of 0.05–0.07 mm width around garnet (Fig. 4b). In this rock, garnet varies from 40% to 45% in volume, with grain size ranging from 0.05 to 3.0–4.0 mm and contain small inclusions of rutile, ilmenite and zircon, and less commonly, inclusions of residual omphacite (Fig. 4c). Garnets have high content of grossular (grs)+andradite (adr) from 23.48% up to 34.65%. End-member components are in the range of $prp_{18.97-27.50}$ $alm_{43.52-49.22}$ $grs_{13.74-32.47}$ $sps_{0.99-3.38}$ (Table 1). In the pyrope-(almandine+spessartine)-grossular ternary diagram (Fig. 5a), garnet analyses plot mainly within the group C eclogite field of Coleman et al. (1965). An example of garnet zoning is shown in Fig. 6. The garnet is rimmed by amphibole and plagioclase kelyphitic rims. The compositional profile shows that garnet is zoned, with prp increasing from core to rim, whereas grs and alm display complementary pattern. This is characteristic of prograde growth zoning (Kienast et al., 1991; O'Brien, 1997). The prp component drops slightly, concomitant with a rise in the grs component near the right rim. This is considered to be a result of retrogradation (Kienast et al., 1991; O'Brien, 1997; Spear and Markussen, 1997). The clinopyroxene includes both omphacite and Na-poor clinopyroxene; the latter intergrown with plagioclase (Fig. 4d). Omphacite occurs as mineral inclusions within garnets and has a jadeite (jd) component of 28.7–29.1 mol%. Some omphacite has degenerated to sodic diopside, with a jd component of 12.05–16.27 mol%, or to amphibole where it was affected by later metamorphism. The Na-poor clinopyroxene, in vermicular symplectite with plagioclase after omphacite, is sodic diopside with a jd component of 3.90–19.48 mol% (Table 1, Fig. 5b). Na-poor clinopyroxenes make up ca. 60 vol.% of the symplectite. The plagioclase intergrowth with Na-poor clinopyroxene is extremely fine-grained (<0.02 mm), and have CaO ranging from 4.56% to 6.35% and 22.0% to 30.7% anorthite (an), whereas in the kelyphitic rim with amphibole around garnet, the plagioclase has a composition of 8.08% CaO and 38.6% an (Table 1). Amphiboles occur as mineral inclusions within garnets or in kelyphitic rims with plagioclase surrounding garnets, and are calcic amphibole based on the classification of Leake (1978). They occur in two forms: (1) the amphiboles within garnet are 0.5 to 1.0 mm in size and classify as ferroan pargasitic hornblende with 6.278 to 6.410 p.f.u of Si and 0.614 to 0.622 of $Mg/(Mg+Fe^{2+})$; and (2) amphiboles in kelyphitic rims around garnet are 0.05 to 0.07 mm in size and classify as magnesio-hastingsite with 6.197 p.f.u of Si and 0.746 of $Mg/(Mg+Fe^{2+})$ and higher Fe^{3+} than ^{VI}Al (Table 1).

Table 1
Representative mineral compositions of weakly amphibolitized eclogites

Sample no.	982212										170421						
	C-Grt	M-Grt	R-Grt	CpxI	CpxI	CpxII	AmpI	AmpII	PlI	PlII	C–Grt	R–Grt	CpxI	CpxI	CpxII	AmpI	PlI
SiO_2	38.51	38.45	38.56	53.51	53.35	54.51	43.75	42.59	61.89	58.03	38.19	38.73	53.88	52.84	52.86	42.65	62.51
TiO_2	0.22	0.00	0.00	0.14	0.14	0.00	0.50	0.22	0.11	0.00	0.10	0.13	0.11	0.06	0.00	0.26	0.00
Al_2O_3	21.40	21.52	21.07	8.39	3.59	1.03	14.11	13.85	24.29	26.19	21.26	21.57	8.08	6.20	6.70	16.76	23.20
FeO	22.55	23.46	23.59	5.28	7.07	7.91	12.89	13.04	0.19	0.08	21.91	21.67	5.61	6.50	6.27	11.85	0.27
MnO	0.72	0.62	1.49	0.07	0.07	0.03	0.18	0.24	0.27	0.00	0.47	0.45	0.02	0.03	0.05	0.07	0.00
MgO	6.94	6.75	5.99	9.04	12.39	13.83	11.37	12.86	0.10	0.06	4.84	5.02	9.91	9.97	9.63	10.57	0.11
CaO	9.61	8.97	8.18	18.83	20.63	22.71	12.60	12.32	6.35	8.08	12.30	12.12	17.31	21.17	21.01	11.87	4.56
Na_2O	0.29	0.45	0.00	3.96	1.94	0.54	2.02	2.44	7.85	7.04	0.08	0.06	4.19	2.15	2.63	3.30	8.94
K_2O	0.00	0.00	0.00	0.00	0.00	0.11	0.11	0.09	0.10	0.08	0.00	0.00	0.00	0.13	0.06	0.23	0.02
Total	100.24	100.22	98.88	99.22	99.18	100.67	97.53	97.65	101.15	99.56	99.15	99.75	99.11	99.05	99.21	97.56	99.61
Si	2.947	2.944	3.023	1.958	1.976	2.009	6.410	6.197	2.722	2.607	2.979	2.999	1.966	1.966	1.956	6.278	2.778
Ti	0.013	0.000	0.000	0.004	0.004	0.000	0.055	0.024	0.004	0.000	0.006	0.008	0.003	0.002	0.000	0.029	0.000
Al	1.928	1.940	1.945	0.361	0.156	0.045	2.435	2.373	1.258	1.386	1.952	1.967	0.347	0.272	0.292	2.906	1.214
Fe^{3+}	0.190	0.233	0.004	0.000	0.024	0.000	0.070	0.638	0.000	0.000	0.085	0.023	0.010	0.000	0.000	0.000	0.000
Fe^{2+}	1.253	1.270	1.543	0.162	0.195	0.243	1.510	0.948	0.007	0.003	1.344	1.380	0.159	0.202	0.194	1.459	0.010
Mn	0.047	0.040	0.099	0.002	0.002	0.001	0.022	0.030	0.010	0.000	0.031	0.030	0.001	0.001	0.002	0.009	0.000
Mg	0.792	0.770	0.700	0.493	0.684	0.759	2.483	2.789	0.007	0.004	0.563	0.579	0.539	0.553	0.531	2.320	0.007
Ca	0.788	0.736	0.687	0.738	0.818	0.897	1.978	1.921	0.299	0.389	1.028	1.005	0.677	0.844	0.832	1.872	0.217
Na	0.043	0.067	0.000	0.281	0.139	0.039	0.574	0.688	0.670	0.613	0.012	0.009	0.297	0.155	0.189	0.942	0.771
K	0.000	0.000	0.000	0.000	0.000	0.005	0.021	0.017	0.006	0.005	0.000	0.000	0.000	0.006	0.003	0.043	0.001
Total	8.001	8.000	8.001	3.999	3.998	3.988	15.572	15.626	4.983	5.007	8.000	8.000	3.999	3.994	4.000	15.857	4.999
jd				28.71	12.05	3.90							29.12	16.27	19.48		
an									30.7	38.6							22.0
grs	17.46	13.74	23.28								30.37	32.47					
prp	27.50	27.36	23.92								18.97	19.39					
alm	43.52	45.08	49.22								45.33	45.98					
sps	1.62	1.43	3.38								1.05	0.99					
adr	9.90	12.39	0.20								4.28	1.17					

C-Grt: Grt core composition, M-Grt: middle Grt composition, R-Grt: Grt rim composition; CpxI: Cpx inclusion in garnet, CpxII: Cpx intergrown with Pl in vermicular symplectite; AmpI: Amp inclusion in garnet, AmpII: Amp in kelyphitic rim around garnet; PlI: Pl intergrown with CpxII in vermicular symplectite, PlII: Pl in kelyphitic rim around garnet; [The mineral abbreviations in this table are after Kretz (1983)]. jd: jadeite component of Cpx; an: anorthite component of Pl; grs, prp, alm, sps, and adr are end-member proportions of Grt. Garnets normalized to 12 oxygens, pyroxenes to 6 oxygens, amphiboles to 23 oxygens and plagioclases to 8 oxygens. The charge balance calculation used for Fe^{3+} in garnet and pyroxene. Fe^{3+} in amphibole calculated for 13 cations excluding Ca, Na and K. Garnet end-members calculation is after Rickwood (1968); Clinopyroxene end-members have been calculated according to the following procedure: (1) ferric iron assigned to aegirine, (2) remaining Na assigned to jadeite, (3) all Ti assigned to titanaugite, (4) remaining Al assigned to Ca-Tschermak's component, (5) remaining Ca assigned to wollastonite, (6) remaining Mg assigned to enstatite, (7) remaining Fe assigned to ferrosilite.

The intensely amphibolitized retrograded eclogite samples were collected from the Zhenningbu, Qilidun and Luhebu villages, and are characterized by extensive development of amphibole and plagioclase, with the absence of omphacite and vermicular symplectite of Na-poor clinopyroxene and plagioclase (Table 2). In this rock, garnet commonly contains inclusions of rutile, ilmenite, amphibole and quartz, and aggregate inclusions of amphibole and plagioclase. They are commonly rimmed by amphibole and plagioclase kelyphitic rims (Fig. 4e,f)). Garnets are locally completely replaced by granular symplectite of amphibole and plagioclase (Fig. 4e). The modal amount of garnets varies from 0% to 40%. Individual grains are mostly 1.0–3.0 mm in diameter. Garnets have contents of grs+adr from 21.98% to 29.61%. Their end-member components are in the range of $prp_{10.48-34.62}$ $alm_{40.89-58.29}$ $grs_{13.19-29.61}$ $sps_{1.70-9.80}$ (Table 2). In the pyrope-(almandine+spessartine)-grossular ternary diagram (Fig. 5a), garnets are plotted mainly within the group C eclogite field or at the boundary between the C and B field of Coleman et al. (1965). Moreover, garnets show different patterns of compositional zoning that implies a complicated metamorphic history. Garnets show prograde (Mg-increasing) zoning in samples 81707 and 819032, whereas some grains such as sample 819038 show retrograde zoning (Table 2). Amphibole occurs as granular symplectite intergrown with plagioclase replacing garnets, kelyphite with plagioclase around garnet, and replacing clinopyroxenes in the matrix. The amount of amphibole is about 50–60 vol.% and is locally more than 60 vol.%. The amphiboles are calcic, ranging from tschermakite, tschermakitic hornblende to magnesio-hornblende, after the classification of Leake (1978). The amount of plagioclase is about 10–40 vol.%. Plagioclase from granular symplectite and kelyphitic rims with amphibole contains 45.5–49.7% of a component, which is less than the an-content (~53.1%) for plagioclase in the matrix.

4. Metamorphic stages and *P–T* estimations

Based on petrographic and mineralogical examination, three main metamorphic stages can be recognized: (1) a peak eclogite facies stage; (2) a high pressure granulite facies stage, and (3) an amphibolite facies stage.

Table 2
Representative mineral compositions of intensely amphibolitized eclogites

Sample No.	81807						819032					819038			82002	
	C-Grt	M-Grt	R-Grt	AmpI	AmpII	PlI	C-Grt	M-Grt	R-Grt	AmpIII	PlII	C-Grt	R-Grt	AmpI	AmpIV	PlIII
SiO_2	38.76	39.73	39.26	43.27	45.44	56.70	38.07	38.24	38.44	48.52	56.33	38.40	37.86	44.02	43.78	54.85
TiO_2	0.20	0.07	0.01	1.14	0.96	0.10	0.05	0.08	0.00	0.82	0.03	0.00	0.00	1.31	1.54	0.00
Al_2O_3	21.37	21.66	21.73	12.18	10.34	27.50	21.62	21.64	22.09	7.49	27.36	21.69	21.99	12.17	12.45	28.28
FeO	22.16	23.55	26.23	16.95	18.00	0.00	23.43	23.42	23.77	14.93	0.38	21.41	25.39	13.70	13.94	0.11
MnO	4.28	1.96	2.08	0.45	0.09	0.00	1.48	0.80	0.69	0.03	0.00	0.82	2.74	0.46	0.07	0.00
MgO	2.60	3.64	3.80	9.43	10.77	0.03	5.39	6.27	7.12	13.71	0.26	8.81	4.55	12.78	11.20	0.16
CaO	10.22	10.29	7.72	11.49	10.70	10.21	10.45	9.64	8.40	12.13	9.60	8.02	7.33	12.16	12.14	11.31
Na_2O	0.30	0.11	0.02	1.34	1.51	5.57	0.05	0.14	0.02	1.03	6.35	0.14	0.00	1.40	1.34	5.31
K_2O	0.00	0.00	0.00	0.90	0.60	0.20	0.00	0.00	0.00	0.02	0.00	0.00	0.00	0.38	0.98	0.32
Total	99.89	101.01	100.85	97.15	98.41	100.31	100.54	100.23	100.53	98.68	100.31	99.29	99.86	98.38	97.44	100.34
Si	3.051	3.077	3.063	6.459	6.598	2.539	2.936	2.942	2.941	6.938	2.528	2.939	2.971	6.342	6.466	2.472
Ti	0.012	0.004	0.001	0.128	0.105	0.003	0.003	0.005	0.000	0.088	0.001	0.000	0.000	0.142	0.171	0.000
Al	1.981	1.975	1.997	2.141	1.769	1.450	1.963	1.960	1.990	1.262	1.446	1.954	2.032	2.065	2.1660	.501
Fe^{3+}	0.000	0.000	0.000	0.450	0.959	0.000	0.161	0.162	0.125	0.679	0.000	0.183	0.020	0.753	0.148	0.000
Fe^{2+}	1.459	1.525	1.712	1.667	1.227	0.000	1.350	1.345	1.396	1.107	0.014	1.187	1.646	0.898	1.573	0.004
Mn	0.285	0.129	0.137	0.057	0.011	0.000	0.097	0.052	0.045	0.004	0.000	0.053	0.182	0.056	0.009	0.000
Mg	0.305	0.420	0.442	2.099	2.331	0.002	0.620	0.719	0.812	2.923	0.018	1.005	0.532	2.745	2.466	0.011
Ca	0.862	0.854	0.645	1.838	1.665	0.490	0.863	0.795	0.689	1.859	0.462	0.658	0.616	1.877	1.921	0.546
Na	0.046	0.017	0.003	0.388	0.425	0.484	0.007	0.021	0.003	0.285	0.553	0.021	0.000	0.391	0.384	0.464
K	0.000	0.000	0.000	0.171	0.111	0.012	0.000	0.000	0.000	0.004	0.000	0.000	0.000	0.070	0.185	0.019
Total	8.001	8.001	8.000	15.397	15.201	4.980	8.000	8.001	8.001	15.148	5.022	8.000	7.999	15.338	15.490	5.017
an						49.7					45.5					53.1
grs	29.61	29.16	21.98				21.22	18.95	19.02			13.19	23.48			
prp	10.48	14.35	15.05				21.15	24.71	30.85			34.62	21.31			
alm	50.11	52.09	58.29				46.08	46.20	41.30			40.89	46.72			
sps	9.80	4.39	4.68				3.30	1.79	1.70			1.83	7.29			
adr							8.25	8.35	7.14			9.46	1.19			

Same abbreviations and calculation methods in Table 1 were used.

4.1. Peak eclogite facies stage

The mineral assemblage of the peak eclogite facies consists of garnet, omphacite and rutile (±quartz), with rare inclusions in garnet; it is characterized by relict omphacite in garnet. Using the conventional Fe–Mg distribution geothermometer for garnet and omphacite (Ravna, 2000a), and the geobarometer based on the jadeitic content of omphacite in the presence of quartz according to the reaction Ab=Jd+Qtz (Holland, 1980, 1983), we estimate peak eclogite facies conditions to be T=680–730 °C and P>1.40–1.50 GPa (minimum pressure estimations). The composition of garnet surrounding omphacite from the weakly amphibolitized eclogite (omphacite-bearing garnet granulite) was used; for omphacite, those occurring as mineral inclusions within garnet with a jadeite component of 28.71–29.12 mol% were utilized.

4.2. Granulite facies stage

The high pressure granulite facies is marked by the decomposition of omphacite, producing a less jadeitic clinopyroxene and plagioclase (Dunn and Medaris, 1989; O'Brien et al., 1992). In the weakly amphibolitized retrograded eclogite, omphacite broke down to a fine-grained vermicular symplectite consisting of clinopyroxene (jd: 3.90–19.48%) and plagioclase (an: 22.0–30.7%), the result is a high pressure granulite facies assemblage of garnet, sodic diopside, plagioclase and titanite (±quartz). Similar textures have been described in altered eclogites in Antarctica (Vincenzo and Palmeri, 2001), China (Yang, 2001), Russia (Smelov and Beryozkin, 1993), East Greenland (Messiga et al., 1990), Germany (O'Brien, 1989), and in other areas where symplectites partially or completely replace omphacite. These vermicular symplectites can be explained by a breakdown of jd-rich clinopyroxene (omphacite), in association with a pre-existing garnet, in the high pressure granulites facies (Dunn and Medaris, 1989; Smelov and Beryozkin, 1993).

4.3. Amphibolite facies stage

The amphibolite facies stage is characterized by the development of amphibole. In this stage, retrogressive transformation is reflected in the formation of amphibole and plagioclase kelyphitic rims around garnets. These, in turn, developed into granular symplectites that replace garnets. Previous symplectites of clinopyroxene and plagioclase are now replaced by symplectites of amphibole and plagioclase, together with amphibolitization of clinopyroxene, and recrystallization of amphibole and plagioclase to form a groundmass. The overall mineral assemblage of this stage is composed of amphibole and plagioclase (±garnet, ±rutile, ±titanite). Using the garnet–amphibole geothermometer (Ravna, 2000b) and garnet–amphibole–plagioclase–quartz geobarometer (Kohn and Spear, 1990), we estimate tempera-

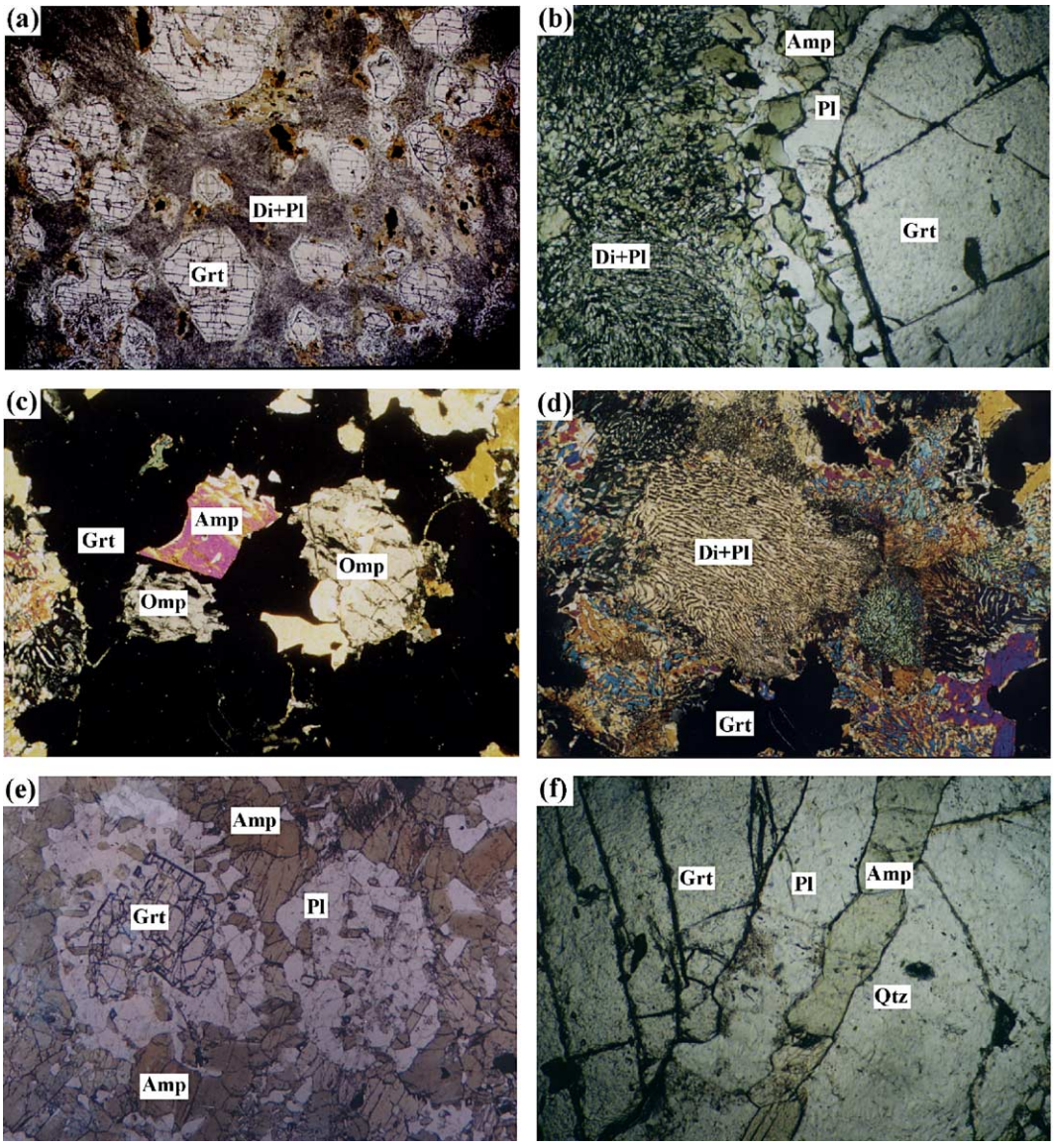

Fig. 4. Photomicrographs of retrograded eclogite textures. Minerals abbreviations are after Kretz (1983). (a) Garnet granulite, mainly consisting of garnet, vermicular symplectite of clinopyroxene and plagioclase in sample 982212 (plane-polarized light), Luhebu. Long dimension is 13 mm. (b) The narrow amphibole and plagioclase kelyphitic rim around garnet in sample 982212 (plane-polarized light), Luhebu. Long dimension is 1.2 mm. (c) Omphacite and amphibole inclusions in garnet and amphibole replaced omphacite in sample 170421 (cross-polarized light), Luhebu. Long dimension is 3 mm. (d) Fine-grained vermicular symplectite of clinopyroxene and plagioclase after omphacite in sample 170421 (cross-polarized light), Luhebu. Long dimension is 3 mm. (e) Kelyphitic rim and pseudomorph of amphibole and plagioclase by granular symplectite after garnet as a result of retrogression in sample 81807 (plane-polarized light), Zhenningbu. Long dimension is 4.8 mm. (f) Kelyphitic rim of amphibole and plagioclase between garnet and quartz in sample 819034 (plane-polarized light), Luhebu. Long dimension is 1.2 mm.

tures of 530–610 °C and pressures to be 0.67–0.81 GPa for this stage.

5. Geochemical and Nd isotope characteristics

Nine retrograded eclogite samples (see Figs. 2 and 3 for sample localities) from Luhebu, Qilidun and Zhenningbu villages were chosen for whole-rock major and trace element and Nd isotope analyses. The results are presented in Tables 3 and 4.

Major element abundances were determined using a Philips PW1400 X-ray fluorescence spectrometer (XRF) at the Institute of Geology and Geophysics, Chinese Academy of Sciences. Analytical uncertainties range from ±1% to ±5% for most of major elements. Trace elements were analyzed using a Finnigan-MAT ELEMENT II inductively coupled plasma mass spectrometer (ICP-MS) at the Analytical and Determining Center, Beijing Research Institute of Uranium Geology. Sample powder (~50 mg) was dissolved in a Teflon bomb using a $HF+HNO_3$ mixture. The Chinese National standard GBW07304 was chosen to calibrate element concentrations in the samples. Analytical precision is ca. ±5% for most of trace elements with abundances ≥20 ppm, and ca. ±10% for those abundances ≤20 ppm. Nd isotope analyses

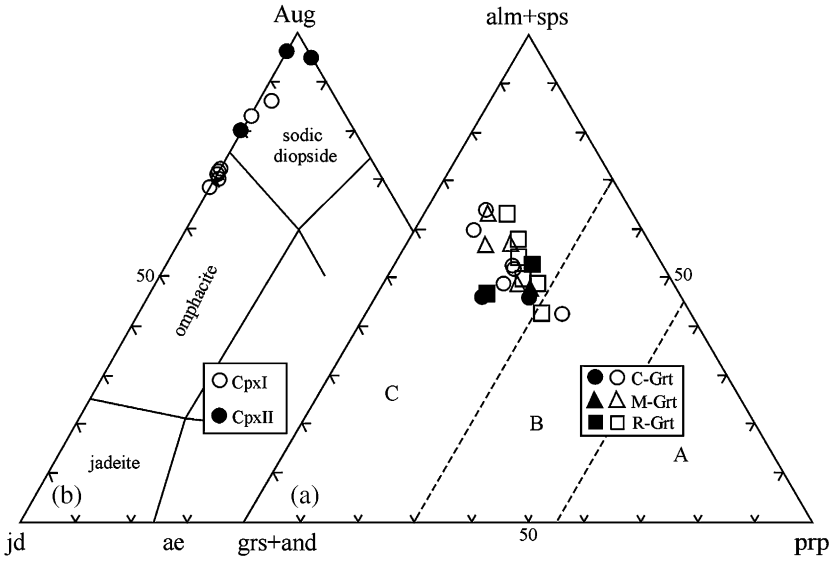

Fig. 5. Representative garnet (a) and pyroxene (b) compositions of the retrograded eclogite plotted after Coleman et al. (1965) and Essene and Fyfe (1967), respectively. 1) CpxI: Cpx inclusion in garnet, CpxII: Cpx intergrown with Pl in vermicular symplectite; 2) C-Grt: Grt core composition, M-Grt: middle Grt composition, R-Grt: Grt rim composition; the open is from the intensely amphibolitized retrograded eclogite, and the solid is from the weakly amphibolitized retrograded eclogite.

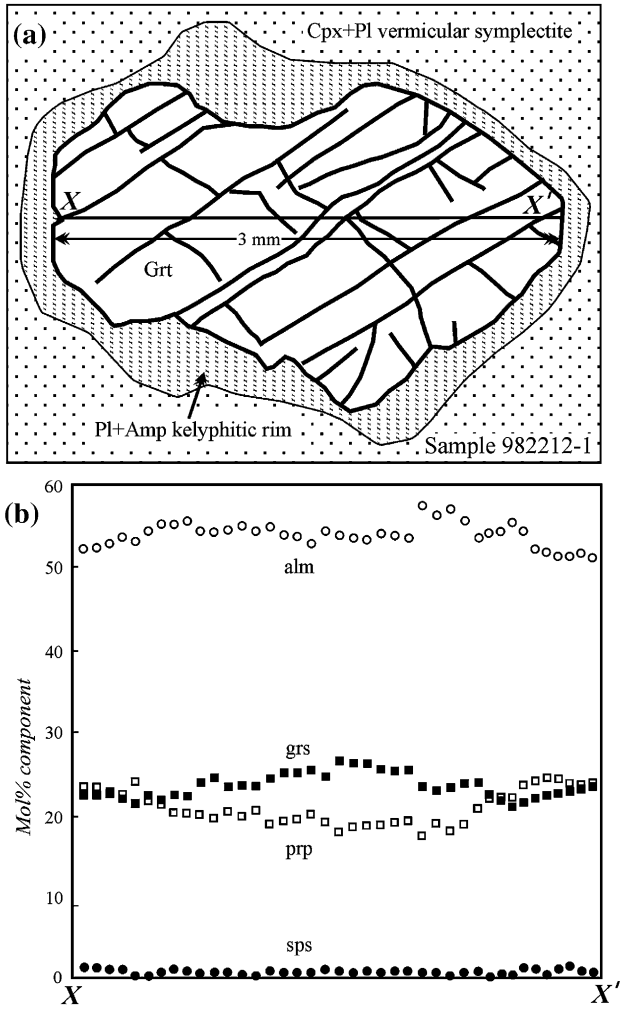

Fig. 6. Compositional profile for garnet from weakly amphibolitized eclogite; (a) map of garnet, (b) compositional profile.

were performed on the VG-354 thermal ionization mass spectrometer at the Isotope Laboratory, Institute of Geology and Geophysics, Chinese Academy of Sciences using standard techniques. Sample dissolution was carried out using acid digestion (HNO_3+HF) in tightly closed Teflon beakers for one week under low temperature. Separation of Sm and Nd was done using AG50W × 8(H^+) cation-exchange column and P507 leaching resin. $^{143}Nd/^{144}Nd$ ratios were normalized against $^{146}Nd/^{144}Nd = 0.7219$. Procedural blanks are 5×10^{-11} g for Sm and Nd. Measurements of the $^{143}Nd/^{144}Nd$ in the La Jolla Nd standard yielded a ratio of 0.511862 ± 0.000003.

The analyzed retrograded eclogite samples display basaltic compositions with SiO_2 ranging from 44.57% to 54.03% and Mg# from 48.68 to 65.34. The range in MgO is from 6.15% to 11.31% and in TiO_2 from 0.92% to 1.70% (Table 3). All analyses were plotted on the SiO_2 versus Nb/Y classification diagram of Winchester and Floyd (1977), most samples show sub-alkaline basaltic compositions (Fig. 7). Sample 819034 with the higher SiO_2 of 54.03% plots within the andesite field. In the SiO_2 versus FeO*/MgO diagram, all samples are clearly tholeiitic in composition (Fig. 8). When plotted on different discrimination diagrams (Fig. 9), all samples fall in the mid-ocean ridge basalt (MORB) or the island arc tholeiite (IAT) field. For example, on the diagrams of $TiO_2/MnO/P_2O_5$ of Mullen (1983, Fig. 9a) and FeO*/MgO versus TiO_2 of Glassley (1974, Fig. 9b), samples from Zhenningbu and Qilidun clearly fall into the IAT and MORB fields, respectively, whilst samples from Luhebu village fall into the field of MORB to IAT. On the V versus Ti diagram of Shervaris (1982, Fig. 9c), sample from Zhenningbu has lower Ti/V of 13.80, consistent with an island-arc tholeiite (IAT), whereas samples with higher values Ti/V of 22.93 to 32.19 from Qilidun lie in the OFB

Table 3
Major and trace element data for retrograded eclogites

Location Sample	Zhenningbu	Luhebu						Qilidun	
	81807	819011	819012	819013	819032	819034	982212	82001	82002
Major elements(%)									
SiO_2	50.45	46.16	44.57	48.53	50.52	54.03	46.67	50.04	48.85
TiO_2	0.92	1.58	1.70	1.08	0.94	1.06	1.54	1.44	1.01
Al_2O_3	13.37	14.82	14.49	15.06	13.71	13.53	15.03	15.97	15.68
Fe_2O_3	2.46	1.43	2.73	1.15	2.26	1.16	1.33	1.85	1.56
FeO	10.85	11.73	11.66	12.77	11.27	11.24	12.52	9.64	7.22
MnO	0.13	0.18	0.17	0.16	0.15	0.13	0.17	0.14	0.13
MgO	7.59	11.31	10.05	7.85	7.18	6.53	7.85	6.15	9.11
CaO	9.71	8.32	9.38	9.84	11.00	8.24	11.47	9.79	11.77
Na_2O	1.61	0.80	1.02	1.16	1.53	1.70	2.01	2.53	1.81
K_2O	0.51	0.85	0.56	0.16	0.10	0.30	0.07	0.74	0.53
P_2O_5	0.07	0.02	0.17	0.10	0.10	0.13	0.02	0.16	0.10
LOI	1.99	2.40	3.06	1.79	1.25	1.57	1.39	1.66	1.78
Total	99.66	99.60	99.56	99.65	100.01	99.62	100.07	100.11	99.55
$Mg^{\#}$	50.90	60.79	55.95	50.36	49.06	48.68	50.52	49.25	65.34
Rare earth element (ppm)									
La	2.31	115.20	6.25	3.87	6.22	2.59	27.73	6.20	2.43
Ce	6.51	237.64	14.82	6.20	12.42	6.45	60.38	13.84	6.97
Pr	0.79	7.58	2.28	1.24	1.73	1.05	7.34	2.36	0.80
Nd	4.58	32.47	11.11	6.16	8.30	5.70	28.76	13.14	4.03
Sm	1.93	6.19	4.01	2.55	2.61	2.47	6.34	4.64	1.56
Eu	0.79	1.66	1.46	0.96	0.93	1.05	1.91	1.80	0.67
Gd	3.06	8.78	7.75	3.56	3.45	4.14	7.46	5.80	2.34
Tb	0.64	1.54	1.58	0.72	0.68	0.83	1.31	1.08	0.51
Dy	4.46	9.57	9.66	5.65	4.85	5.55	8.26	7.10	3.63
Ho	0.98	2.01	1.92	1.37	1.09	1.22	1.74	1.45	0.81
Er	3.16	5.94	5.53	4.25	3.50	3.81	5.20	4.47	2.41
Tm	0.46	0.89	0.76	0.63	0.52	0.56	0.76	0.64	0.35
Yb	3.17	5.94	5.01	4.20	3.52	3.76	5.02	4.13	2.24
Lu	0.50	0.91	0.73	0.66	0.54	0.58	0.76	0.61	0.33
Y	26.80	56.40	52.50	36.28	29.90	32.56	47.15	36.62	20.84
Trace element (ppm)									
Sc	67.45	55.26	62.17	73.44	69.41	63.87	61.36	64.08	48.45
V	400.12	202.05	393.32	333.49	413.84	352.77	334.93	268.20	264.20
Cr	61.02	258.34	194.54	92.96	61.49	45.73	154.85	119.97	196.22
Co	56.94	46.05	39.37	40.80	51.69	51.16	46.57	52.91	46.55
Ni	89.57	367.11	245.86	113.93	87.42	95.40	188.40	127.31	137.43
Rb	6.90	29.48	20.97	5.79	3.08	11.64	3.38	27.23	15.25
Sr	62.10	80.55	99.76	53.92	62.00	121.16	119.97	780.94	182.69
Cs	0.27	0.39	0.93	0.30	0.14	0.40	0.27	0.60	0.49
Ba	67.19	127.22	113.75	40.49	15.82	29.52	18.76	77.49	85.71
Zr	58.94	200.01	142.88	66.84	70.12	70.32	92.25	85.02	48.94
Hf	2.21	9.01	5.31	3.15	2.01	1.82	2.44	3.69	1.12
Nb	1.10	21.40	17.79	6.56	1.38	1.61	15.86	3.54	1.81
Ta	0.56	2.81	2.01	0.91	0.52	0.40	1.62	1.06	0.18
U	0.22	0.92	0.44	0.45	0.21	0.25	1.18	0.66	0.18
Th	1.07	17.86	1.48	0.45	0.32	0.17	13.44	0.86	0.17

$Mg^{\#}=Mg/(Mg+TFe^{2+})$.

and BAT (MORB) field. Samples from Luhebu village have Ti/V values ranging from 13.62 to 46.88, falling in the field of MORB to IAT. On the Zr/Y versus Zr diagram of Pearce and Norry (1979), most samples are intermediate between MORB and IAB (island arc basalt), with the exception of samples 819011 and 819012 with higher values Zr/Y of from 2.72 to 3.55. The transitional IAT/MORB character of the retrograded eclogites suggests that their magmatic precursors were likely formed in an eruptive environment of the ophiolitic sequence (Hussein et al., 2004).

Three types of retrograded eclogite are recognized by their REE abundances and pattern (Table 3 and Fig. 10a). The first type (four samples) is LREE-depleted with chondrite-normalized $(La/Yb)_N$ of 0.46–0.73 and total REEs of 29.08–42.02 ppm [(10–15) × chondrite values]. The four samples show no Eu anomaly (Eu/Eu*=0.97–1.07). This kind of REE distribution is very similar to patterns of

Table 4
Sm–Nd isotopic data for retrograded eclogites from Chicheng

Sample	Locality	Sm(ppm)	Nd(ppm)	$^{147}Sm/^{144}Nd$	$^{143}Nd/^{144}Nd$	$\pm 2\sigma$	$f_{Sm/Nd}$	$\varepsilon_{Nd}(0)$	$\varepsilon_{Nd}(t)$
81807	Zhenningbu	1.90	4.18	0.2742	0.513202	12	0.39	11.00	6.67
819011	Luhebu	6.06	31.76	0.1155	0.512137	10	−0.41	−9.77	−5.43
819012	Luhebu	3.90	10.72	0.2202	0.512508	9	0.12	−2.54	−3.86
819013	Luhebu	2.32	5.79	0.2420	0.512594	8	0.23	−0.86	−3.40
819032	Luhebu	2.95	7.71	0.2317	0.512623	11	0.18	−0.29	−2.25
819034	Luhebu	2.36	5.46	0.2621	0.512896	12	0.33	5.03	1.37
982212	Luhebu	6.24	28.16	0.1340	0.512187	9	−0.32	−8.80	−5.29
82001	Qilidun	3.94	11.25	0.2120	0.513060	11	0.08	8.23	7.38
82002	Qilidun	1.41	3.85	0.2225	0.513221	9	0.13	11.37	9.94

The following constants have been used in the calculation: the present-day CHUR values are $^{143}Nd/^{144}Nd=0.512638$ and $^{147}Sm/^{144}Nd=0.1967$, $\lambda^{147}Sm=6.54\times10^{-12}$/year, $t=438$ Ma.

MORB (Sun and McDonough, 1989). The second type (three samples) is a flat REE pattern with $(La/Yb)_N$ of 0.84–1.19 and total REEs of 50.36–72.87 ppm [about 20 × chondrite values], similar to those of transitional MORB (Sun and McDonough, 1989). The three samples show either a weak negative or slightly positive Eu anomaly (Eu/Eu*=0.79–1.06). The third type (two samples) is LREE-enriched with $(La/Yb)_N$ of 3.72–13.08 and high total REEs of 162.97–436.32 ppm. These samples show a small but distinct negative Eu anomaly (Eu/Eu*=0.69–0.85).

Fig. 10b shows MORB-normalized trace element patterns (Pearce, 1982) for the above three types of retrograded eclogites. The two types of retrograded eclogite samples with LREE-depleted or nearly flat REE patterns show approximately the same abundance of High Field Strength Elements (HFSE) to average MORB, but the third type has higher Th, Nb, Ta, Zr, Hf and Y, and lower P relative to the first type. The enrichment of Nb and Ta in the third type may indicate crustal contamination.

The retrograded eclogite samples from Zhenningbu and Qilidun have LREE depleted or nearly flat REE patterns. These show relatively high positive $\varepsilon_{Nd}(t)$ values of +6.67 to+9.94 (Table 4; Fig. 11), which suggests an oceanic affinity. Samples from Luhebu village can be classified into three types by their Nd isotope. The first type shows lower positive $\varepsilon_{Nd}(t)$ (+1.37) and $f_{Sm/Nd}$ values (+0.33) (sample 819034), which reveals an oceanic affinity and addition of minor crustal components. The second type (three samples) has relatively low $f_{Sm/Nd}$ values of +0.12 to +0.23 and negative $\varepsilon_{Nd}(t)$ values of −2.25 to −3.86, and similar to those of eclogites from Hercynian belt of western Europe which resulted from crustal contamination by reinjection of crustal rocks (Jahn, 1999). In the $\varepsilon_{Nd}(0)$ versus $^{147}Sm/^{144}Nd$ and $\varepsilon_{Nd}(t)$ versus $^{147}Sm/^{144}Nd$ diagrams, these samples plotted within the field of Hercynian belt of western Europe (Fig. 11), which reveals more crustal contamination relative to the first type. The third type(two samples) is characterized by negative $\varepsilon_{Nd}(t)$ (from −5.29 to −5.43) and $f_{Sm/Nd}$ values (from −0.32 to −0.41) (Table 4). Two possibilities account for their origin; either a continental affinity or crustal contamination. In the $\varepsilon_{Nd}(0)$ versus $^{147}Sm/^{144}Nd$ and $\varepsilon_{Nd}(t)$ versus $^{147}Sm/^{144}Nd$ diagrams (Fig. 11), these samples plot at the boundary between the Dabie terrane and Hercynian belt of western Europe. In addition, eclogites from the Dabie and

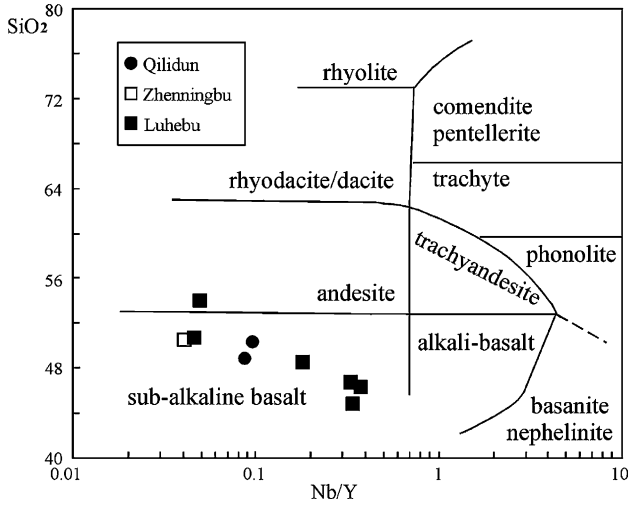

Fig. 7. SiO_2 versus Nb/Y diagram showing the field of the retrograded eclogite. Field boundaries after Winchester and Floyd (1977).

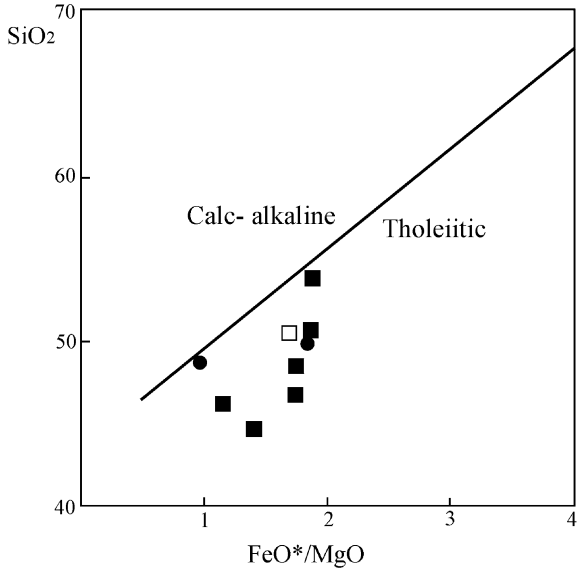

Fig. 8. SiO_2 versus FeO*/MgO diagram for the retrograded eclogite. Index is same as Fig. 7. Field boundary after Miyashiro (1975).

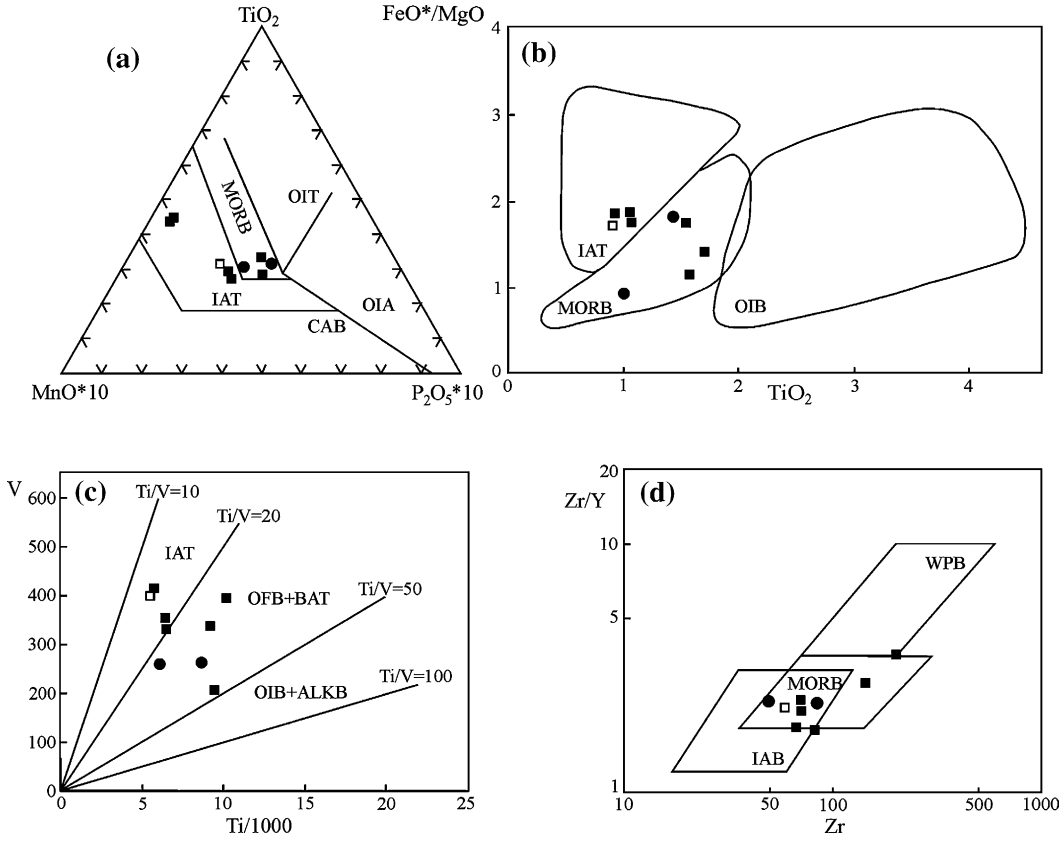

Fig. 9. Samples plotted on various discriminant diagrams. Index is same as Fig. 7. The abbreviations are as follows: MORB, mid-ocean rodge basalts; IAT: island-arc tholeiites; OIT: ocean-island tholeiites; OIA: ocean-island alkalic basalts; CAB: calc-alkaline basalts; OFB: ocean floor basalts; BAT: back-arc basin tholeiites; WPB: within plate basalts; IAB: island-arc basalts; OIB: ocean-island basalts; ALKB: alkalic basalts. Discriminant diagrams are from the following sources: $TiO_2/MnO/P_2O_5$ from Mullen (1983), FeO*/MgO versus TiO_2 from Glassley (1974); V versus Ti from Shervaris (1982), and Zr/Y versus Zr from Pearce and Norry (1979).

Sulu terranes have highly negative $\varepsilon_{Nd}(t)$ values −6 to −20) at the time of peak metamorphism or continental collision (~220 Ma) (Jahn, 1999). These values are distinctly different from those of the retrograded eclogite samples in this study. Therefore, the latter may be interpreted as resulting from extensive crustal contamination.

6. SHRIMP U–Pb zircon geochronology

The zircons for our SHRIMP U–Pb geochronological study were separated from two samples, both from Luhebu village. Sample 170411 is weakly amphibolitized whereas sample 819034 is intensely amphibolitized (see Fig. 3 for sample localities).

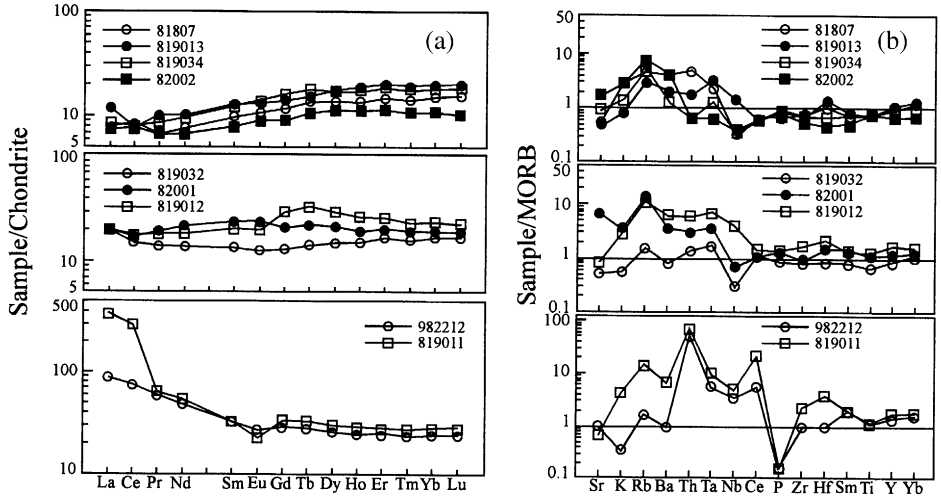

Fig. 10. Chondrite-normalized REE plots for retrograded eclogite samples (a) and MORB-normalized trace element (b) patterns for retrograded eclogite. Normalizing values of chondrite after Boynton (1984) and MORB after Pearce (1982).

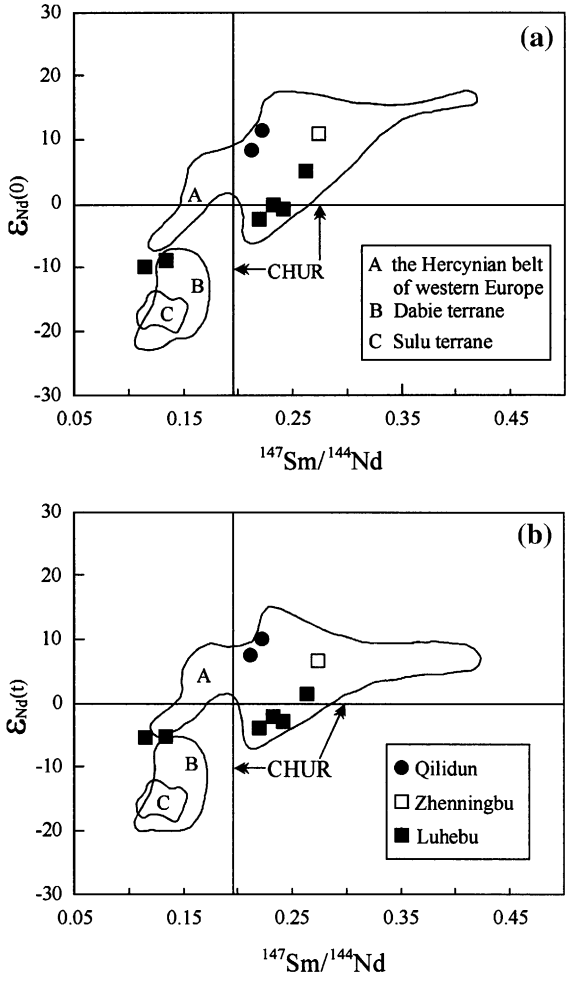

Fig. 11. $\varepsilon_{Nd}(0)$ versus $^{147}Sm/^{144}Nd$ (a) and $\varepsilon_{Nd}(t)$ versus $^{147}Sm/^{144}Nd$ (b) plots for retrograded eclogite. Nd isotopic field of eclogites from the Hercynian belt of western Europe, Dabie terrane and Sulu terrane after Jahn (1999).

The zircon grains from sample 170411 are buff to pale-brown in color, well-formed, elongate crystals with developed prisms, no obvious crack and higher transparency and an average length to width of 2:1. Cathodoluminescence images reveal that most zircon grains are concentrically zoned with very narrow overgrowths at grain margins (Fig. 12a,b,c). This overgrowth rim may have grown during retrogradation. The sample 819034 contains a population of buff zircon crystals with an average length to width ratio of 2.5:1. The crystals show essentially the same morphology as those in sample 170411 (Fig. 12d,e,f).

U–Pb analyses were performed on the SHRIMP II ion microprobe using standard techniques at the Institute of Geology, Chinese Academy of Geological Sciences. Analytical procedures and methods have been described by Williams (1998) and Song et al. (2002). Zircons were mounted in an epoxy resin target together with pieces of the SHRIMP standard zircon (TEM, 417 Ma) so that the standard could be checked frequently and conveniently to monitor instrument stability and ion count. The SHRIMP analytical data for U, Th and Pb are the mean values of five consecutive cycles through the mass stations analyses for each analysis spot. The corresponding isotopic data were calculated using the Ludwing SQUID 1.0 and ISOPLOT program (Ludwig, 1999, 2001). The analytical results are presented in Table 5. The isotope ratios and apparent age uncertainties are given at 1 sigma confidence level. Due to the small amount of ^{207}Pb formed in young (i.e. <1000 Ma) zircons resulted in low count rates and high analytical uncertainties. Thus the determination of the ages for young zircons has to be based primarily on their $^{206}Pb/^{238}U$. The mean $^{206}Pb/^{238}U$ age is 95% at the confidence level shown in Table 5.

A total of 16 analyses were made on 14 zircon grains for sample 170411 along with 5 analyses on the TEM zircon standard. In this sample the analytical point 9.2 reveals a high Th/U value (0.14) and a $^{206}Pb/^{238}U$ age of 438±11 Ma (Table 5). This analytical spot 9.2 is in the core of same zircon with spot 9.1 which give 321±7.3 Ma age (Fig. 12e). Therefore, we infer that it may be an inherited zircon. The higher Th/U value (>0.1) indicates that this zircon is formed through typical of magmatic crystallization (Liu et al., 2003). Thus the $^{206}Pb/^{238}U$ age may be interpreted as the magmatic protolith age of the retrograded eclogite. Spot 6.1 shows a higher Th/U value (0.07) and a lower $^{206}Pb/^{238}U$ age of 298.7±7.0 Ma. Since this zircon grain has many cracks and the analyzed spot lies over these, it may be the Pb loss resulted in reduction of the SHRIMP age. The remaining 14 analyses have a similar range of Th/U values (0 to 0.02) and $^{206}Pb/^{238}U$ age, and yield a weighted mean age of 325±4 Ma, with an MSWD of 1.09 (Fig. 13a). For sample 819034, a total of 13 analyses were carried out on 12 zircon grains, along with 5 analyses on the TEM zircon standard. The 13 analyses have a similar range of Th/U values (0.01 to 0.02) and $^{206}Pb/^{238}U$ ages, and yield a mean age of 325±6 Ma, with an MSWD of 1.49 (Fig. 13b).

7. Discussion and conclusions

7.1. Nature and age of the protoliths

Considering the whole rock composition, K, Na and the low field strength elements (LFSE: Cs, Rb, Sr and Ba) are likely to be remobilized during amphibolite facies or higher grades of metamorphism (Humphris and Thompson, 1978). Due to low solubility in H_2O fluids and refractory properties, the REE and Nd isotope tracers may provide better information about the nature of the retrograded eclogites protoliths (Bernard-Griffiths and Cornichet, 1985; Jahn, 1999). Thus, only immobile elements such as the high-field-strength elements (HFSE: Ti, Zr, Y, Nb, Ta and Hf), REE and Nd isotopes are used in the following discussion to characterize the magmatic affinity of the protolith for retrograded eclogite.

Geochemical studies of the nine retrograded eclogite samples in this paper indicate a tholeiitic protolith composition. The geochemical characteristics are similar to present-day mid-ocean ridge (MORB) or island arc tholeiite (IAT). For example, the characteristics of HFSE are similar to those of MORB, and REE distributions are mainly LREE-depleted or have a nearly flat pattern. The pattern of LREE-enrichment may be due to the influence of a crustal component (Paquette et al., 1989).

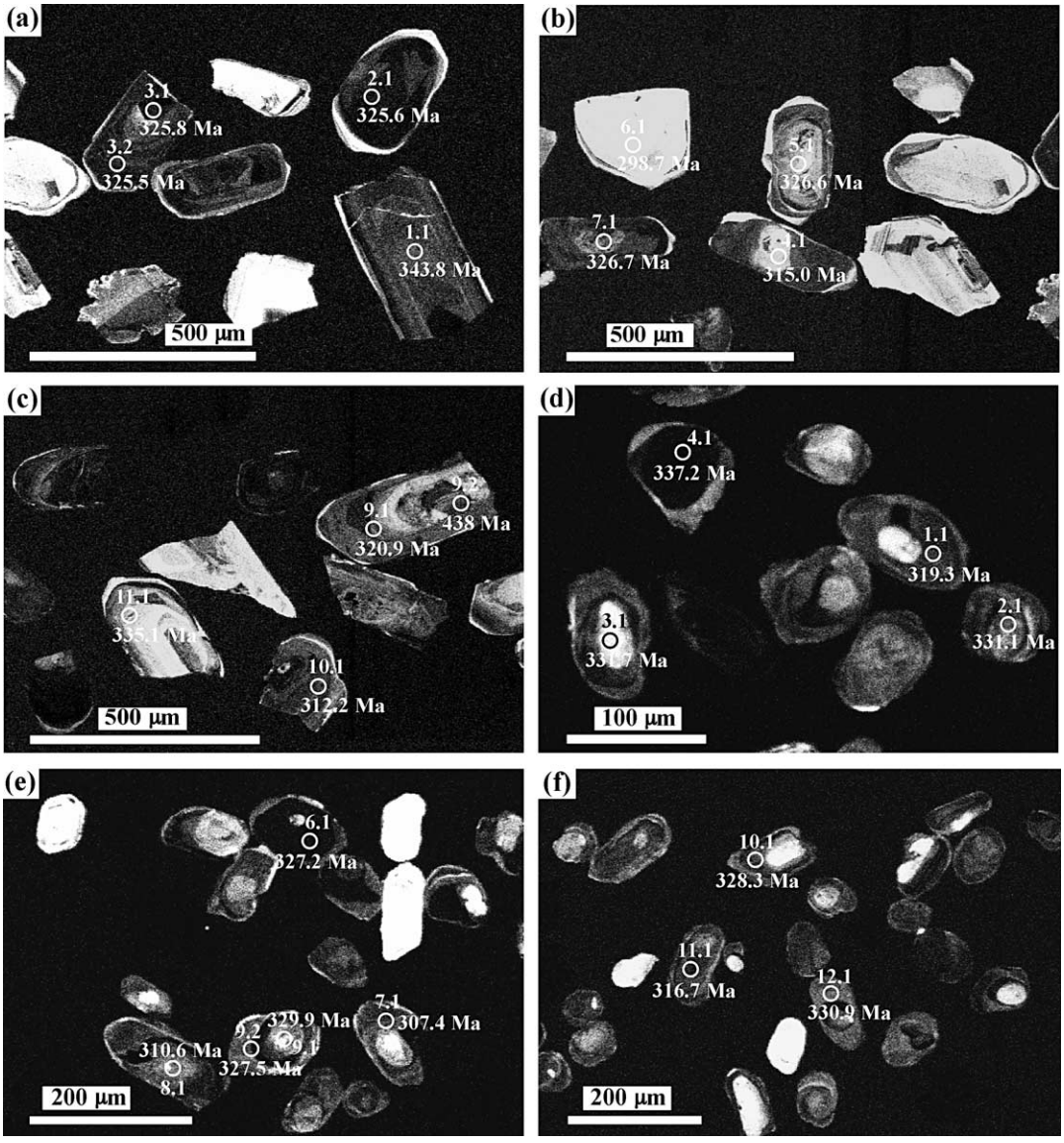

Fig. 12. Cathodoluminescence (CL) images of analyzed zircons from the retrograded eclogite of Chicheng [Samples 170411(a, b and c) and 819034 (d, e and f)]. The dark circles represent the sites of analyzed points. SHRIMP ages depicted are $^{206}Pb/^{238}U$ ages.

Moreover, the Nd isotopes of the nine analyzed samples are also similar to those of MORB, characterized by mainly positive to slightly negative $\varepsilon_{Nd}(t)$ values, providing further evidence that their igneous precursor was oceanic basalt, the product of partial melting of the depleted mantle, to which minor crustal components were added during the subsequent subduction to form eclogitic facies high-pressure metamorphic rocks. The $^{206}Pb/^{238}U$ age of 438 Ma from an inherited magmatic zircon core in sample 170411 implies that this may be the age of the igneous precursor (Table 5). However, more data are required to constrain this age.

7.2. Age of peak eclogite facies metamorphism

SHRIMP zircon isotopic dating of two different textural retrograded eclogite samples give the same mean age of ~325 Ma. The low Th/U (0.01–0.02) values are typical of zircon that has been recrystallized during metamorphism (Liu et al., 2003). According to some authors, when the protolith is a volcanic rock, most of the zircons were formed during the eclogite facies metamorphism (Gebauer and Lappin, 1985; Vidal and Hunziker, 1985).

In addition, petrographical observations show that most of the zircons are included within garnet, along with inclusions of omphacites (jd: 27.95 to 32.05 mol%). Therefore, this age of ~325 Ma closely approaches the time of peak eclogite facies metamorphism. The overgrowth of zircon is unfortunately too narrow for SHRIMP analysis, so the age of retrograde metamorphism remains unconstrained.

7.3. Tectonic implications of the retrograded eclogite

To the southwest of the Chicheng, retrograded eclogite has been discovered at Baimashi near Heng Mountains in the NCC

Table 5
SHRIMP U–Pb data of zircons in sample 170411 and 819034 from retrograded eclogites

Spot	^{206}Pbc (%)	U (ppm)	Th (ppm)	Th/U	^{206}Pb* (ppm)	^{204}Pb/ ^{206}Pb	^{207}Pb*/ ^{206}Pb*	±%	^{207}Pb*/ ^{235}U	±%	^{206}Pb*/ ^{238}U	±%	^{206}Pb*/^{238}U* age (Ma)	^{207}Pb*/^{206}Pb* age (Ma)
Sample 170411														
1.1	0.29	322	6	0.02	15.2	0.00016	0.0545	3.0	0.412	3.9	0.0548	2.4	343.8±8.0	393±68
2.1	0.21	645	4	0.01	28.8	0.00012	0.05214	1.8	0.372	2.9	0.0518	2.3	325.6±7.3	291±41
3.1	0.73	439	3	0.01	19.7	0.00040	0.0483	3.7	0.345	4.4	0.0518	2.3	325.8±7.4	115±88
3.2	0.44	469	6	0.01	21.0	0.00024	0.0501	3.8	0.358	4.5	0.0518	2.3	325.5±7.4	199±89
4.1	1.20	136	1	0.01	5.92	0.00066	0.0479	12	0.331	12	0.0501	2.6	315.0±7.9	96±290
5.1	–	170	1	0.00	7.55	−0.00020	0.0584	4.5	0.418	5.1	0.0520	2.4	326.6±7.7	543±98
6.1	0.57	408	30	0.07	16.7	0.00031	0.0525	4.7	0.344	5.3	0.0474	2.4	298.7±7.0	309±110
7.1	0.79	68	0	0.00	3.05	0.00043	0.0542	11	0.389	12	0.0520	2.8	326.7±8.9	380±260
8.1	0.81	133	1	0.00	5.99	0.00044	0.0511	8.2	0.367	8.5	0.0521	2.5	327.5±8.1	246±190
9.1	0.48	346	1	0.00	15.3	0.00026	0.0508	3.5	0.357	4.2	0.0510	2.3	320.9±7.3	230±81
9.2	0.32	434	59	0.14	26.3	0.00018	0.0761	2.0	0.738	3.2	0.0703	2.5	438±11	1098±40
10.1	0.19	297	4	0.01	12.7	0.00011	0.0523	3.1	0.358	3.9	0.0496	2.4	312.2±7.2	299±72
11.1	1.92	108	0	0.00	5.03	0.0011	0.0413	15	0.304	16	0.0534	2.7	335.1±8.7	−269±390
12.1	4.01	41	0	0.00	1.81	0.0022	0.0460	34	0.31	34	0.0496	3.5	312±11	−5±830
13.1	0.19	677	8	0.01	30.7	0.00010	0.05318	1.7	0.386	2.9	0.0526	2.3	330.3±7.4	337±38
14.1	0.35	580	6	0.01	25.7	0.00019	0.0503	2.4	0.357	3.3	0.0515	2.3	323.8±7.3	209±55
Sample 819034														
1.1	0.86	247	4	0.02	10.9	0.00047	0.0520	7.0	0.364	7.4	0.0508	2.4	319.3±7.5	286±160
2.1	0.43	288	5	0.02	13.1	0.00024	0.0535	4.4	0.388	5.1	0.0527	2.5	331.1±8.2	348±100
3.1	0.68	340	7	0.02	15.5	0.00037	0.0523	3.5	0.380	4.2	0.0528	2.3	331.7±7.6	297±80
4.1	0.10	1216	20	0.02	56.2	0.000057	0.05215	1.6	0.386	2.8	0.0537	2.3	337.2±7.5	292±36
5.1	0.28	220	3	0.01	10.1	0.00015	0.0523	3.2	0.379	4.0	0.0526	2.4	330.2±7.7	299±74
6.1	0.28	590	8	0.01	26.5	0.00015	0.0520	2.4	0.374	3.4	0.0521	2.3	327.2±7.4	287±56
7.1	0.60	241	3	0.01	10.2	0.00033	0.0512	4.9	0.345	5.4	0.0488	2.4	307.4±7.2	252±110
8.1	0.12	260	6	0.02	11.0	0.000066	0.0534	2.6	0.364	3.5	0.0494	2.4	310.6±7.2	346±60
9.1	1.09	251	4	0.02	11.4	0.00060	0.0456	5.4	0.330	5.9	0.0525	2.4	329.9±7.7	−24±130
9.2	0.14	957	13	0.01	42.9	0.000075	0.05165	1.6	0.371	2.8	0.0521	2.3	327.5±7.3	270±36
10.1	0.31	655	12	0.02	29.5	0.00017	0.0506	2.0	0.365	3.1	0.0522	2.3	328.3±7.4	225±47
11.1	0.11	208	3	0.01	9.0	0.000060	0.0549	3.8	0.381	4.5	0.0504	2.4	316.7±7.5	408±84
12.1	0.21	510	12	0.02	23.1	0.00012	0.0526	2.0	0.382	3.1	0.0527	2.4	330.9±7.5	313±46

Errors are 1-sigma level; ^{206}Pbc and ^{206}Pb* indicate the common and radiogenic portions, respectively. Common Pb corrected using measured ^{204}Pb.

(Zhai et al., 1996) (Fig. 1c). The field characteristics, geochemical and protolith features, and the peak-metamorphic age of the retrograded eclogites at Baimashi are entirely different from those of the retrograded eclogites discussed in this paper.

The Baimashi retrograded eclogites have a peak metamorphic age of either 2500 or 1800 Ma and occur as separate lenses within TTG orthogneisses; they also have protolith features resembling continental gabbroic rock (Guo et al., 1999; Zhai et al., 1996; Zhao et al., 2001; O'Brien et al., 2005). The retrograded eclogites of this study occur within amphibolite facies paragneiss of the Paleoproterozoic Hongqiyingzi Complex, and their protoliths are of oceanic crust MORB or IAT, which underwent eclogite facies metamorphism at ~325 Ma. In addition, these two kinds of retrograded eclogites and their country rocks are separated by the Jining–Congli–Chicheng fault belt (Fig. 1c). Therefore, the Baimashi and Chicheng retrograded eclogites belong to different geological terrains.

The localities of retrograded eclogite in this study are distributed only 100 km south to the boundary of the Paleo-Asian Ocean tectonic region (Fig. 1b), and it is definitely possible that the retrograded eclogites were related to the Paleo-Asian Ocean. A possible scenario is that the eclogite resulted from southward subduction of Paleo-Asian oceanic crust which then underwent high-pressure metamorphism at eclogite facies during subduction. The rocks were then exhumed and moved along the Jining–Shangyi–Congli–Chicheng fault belt. The report of ~438 Ma ancient oceanic crust (435 to 446 Ma) (Zhang and Zhou, 2001) in the Paleo-Asian Ocean tectonic region supports our conclusion.

The retrograded eclogites in this study are thus different from the Precambrian retrograded eclogites within the NCC and may be related to Paleo-Asian oceanic lithosphere evolution during the Late Paleozoic.

Acknowledgements

This study was financially supported by the National Natural Science Foundation of China (Grant No. 40234050, 40472041) and the Chinese Academy of Sciences (Grant No. KZCX1-07). We sincerely thank Prof. D.Y. Liu, P. Jian and Y.S. Wan for their help and discussions on the SHRIMP zircon U–Pb analyses, and J.H. Guo and H.F. Zhang for numerous discussions about the manuscript with

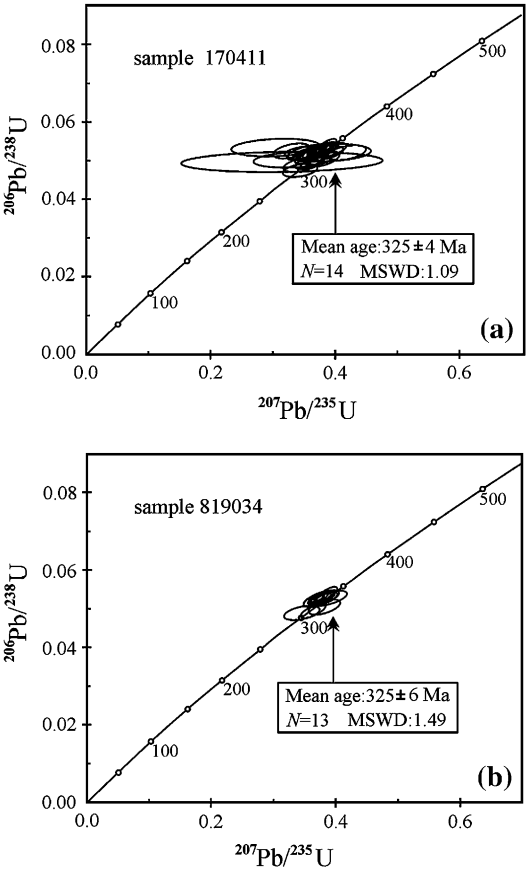

Fig. 13. Concordia plot showing zircon analysis from samples 170411 (a) and 819034 (b).

us. We also thank S.A. Wilde, R.N. Abbott Jr. and C.W. Oh for constructive and helpful comments on the manuscript.

References

Bernard-Griffiths, J., Cornichet, J., 1985. Origin of eclogites from south Brittany, France: an Sm–Nd isotopic and REE study. Chem. Geol. 52, 185–201.

Boynton, W.V., 1984. Geochemistry of rare earth elements: meteorite studies. In: Henderson, P. (Ed.), Rare Earth Element Geochemistry. Elsevire Scientific Publishing Company, Amsterdam, pp. 63–114.

Coleman, R.G., Lee, D.E., Beatty, L.B., Brannock, W.W., 1965. Eclogites and eclogites: their differences and similarities. Geol. Soc. Amer. Bull. 76, 483–508.

Dunn, S.R., Medaris, L.G., 1989. Retrograded eclogites in the Western Gneiss Region, Norway, and thermal evolution of the portion of the Scandianvian Caledonians. Lithos 22, 229–245.

Essene, E.J., Fyfe, W.S., 1967. Omphacite in the California metamorphic rocks. Contrib. Mineral. Petrol. 15, 1–23.

Gebauer, D., Lappin, J.G., 1985. The age and origin of some Norwegian eclogites: a U–Pb zircon and REE study. Chem. Geol. 52, 227–248.

Glassley, W., 1974. Geochemistry and tectonics of the crescent volcanic rocks, Olympic Peninsula, Washington. Geol. Soc. Amer. Bull. 85, 785–794.

Guo, J.H., Zhai, M.G., Li, J.H., Li, Y.G., 1996. Nature of the Early Precambrian Sanggan structure zone in North China Craton: evidence from rock association. Acta Pet. Sin. 12, 193–207. (in Chinese).

Guo, J.H., Zhai, M.G., Li, Y.G., Li, J.H., 1999. Metamorphism, P–T paths and tectonic significance of garnet amphibolite and granilite from Hengshan, North China Craton. Sci. Geol. Sin. 34, 311–325. (in Chinese).

Guo, J.H., Sun, M., Chen, F.K., Zhai, M.G., 2005. Sm–Nd and SHRIMP U–Pb zircon geochronology of high-pressure granulites in the Sanggan area, North China Craton: timing of Paleoproterozoic continental collision. J. Asian Earth Sci. 24, 629–642.

Holland, T.J.B., 1980. The reaction albite=jadeite+quartz determined experimentally in the range 600–1200 °C. Am. Mineral. 65, 129–134.

Holland, T.J.B., 1983. The experimental determination of activities in the disordered and short-range ordered jadeotic pyroxenes. Contrib. Mineral. Petrol. 82, 214–220.

Hu, X.W., Zhang, J.M., Quan, H., 1996. The isotopic ages of the Hongqiyingzi Group in Northern Hebei and its age assignment. Reg. Geol. China 23, 186–192 (in Chinese).

Humphris, S.E., Thompson, G., 1978. Hydrothermal alteration of oceanic basalts by seawater. Geochim. Cosmochim. Acta 42, 107–125.

Hussein, I.M., Kröner, A., Reischmann, T., 2004. The Wadi Onib mafic-ultramafic complex: a Neoproterozoic supra-subduction zone ophiolite in the northern Red Sea hills of the Sudan. In: Kusuy, T.M. (Ed.), Precambrian Ophiolites and Related Rocks. Elsevier B.V, Amsterdam, pp. 163–206.

Jahn, B.M., 1999. Sm–Nd isotope tracer of UHP metamorphic rocks: implications for continental subduction and collisional tectonics. Int. Geol. Rev. 41, 859–885.

Kienast, J.R., Lombardo, B., Biino, G., Pinardon, J.L., 1991. Petrology of very-high-pressure eclogitic rocks from the Brossacsco–Isasca complex, Dora-Maira Massif, Italian Western Alps. J. Metamorph. Geol. 9, 19–34.

Kohn, M.J., Spear, F.S., 1990. Two new geobarometers for garnet amphibolites, with applications to southeastern Vermont. Am. Mineral. 75, 89–96.

Kretz, R., 1983. Symbols for rock-forming minerals. Am. Mineral. 68, 277–279.

Kusky, T.M., Li, J.H., 2003. Paleoproterozoic tectonic evolution of the North China Craton. J. Asian Earth Sci. 22, 23–40.

Leake, B.E., 1978. Nomenclature of amphiboles. Mineral. Mag. 42, 533–563.

Li, J.H., Kroner, A., Qian, X.L., O'Brien, P., 2000. Tectonic evolution of an Early Precambrian high-pressure granulite belt in the North China Craton. Acta Geol. Sin. 74, 246–258.

Liu, D.Y., Jian, P., Zhang, Q., Zhang, F.Q., Shi, Y.R., Shi, G.H., Zhang, N.Q., Tao, H., 2003. SHRIMP dating of adakites in the Tulingkai ophiolite, Inner Mongolia: evidence for the Early Paleozoic subduction. Acta Geol. Sin. 77, 317–327 (in Chinese).

Ludwig, K.R., 1999. Using Isoplot/ EX, Version 2, a Geochronological Toolkit for Microsoft Excel, Berkeley Geochronological Center Special Publication vol. 1a, p. 47.

Ludwig, K.R., 2001. Squid 1.02: A User Manual, Berkeley Geochronological Center Special Publication, vol. 2, p. 19.

Messiga, B., Tribuzio, R., Vannucci, R., 1990. Mafic and ultramafic pods with eclogitic relics from the Proterozoic Nagssugtoqidian mobile belt of east Greenland. Lithos 25, 101–118.

Miyashiro, A., 1975. Classification, characteristics, and origin of ophiolites. J. Geol. 83, 249–281.

Mullen, E.D., 1983. $MnO/TiO_2/P_2O_5$: a minor element discriminant for basaltic rocks of oceanic environments and its implications for petrogenesis. Earth Planet. Sci. Lett. 62, 53–62.

O'Brien, P.J., 1989. The petrology of retrograded eclogites of the Oberpfalz Forest, northeastern Bavaria, West Germany. Tectonophy 157, 195–213.

O'Brien, P.J., 1997. Garnet zoning and reaction textures in overprinted eclogites, Bohnmian Massif, European Variscides: a record of their thermal history during exhumation. Lithos 41, 119–133.

O'Brien, P.J., Rohr, C., Okrusch, M., Patzak, M., 1992. Eclogite facies relics and a multistage breakdown in metabasites of the KTB pilot hole, NE Bavaria: implications for the Variscan tectono-metamorphic evolution of the NW Bohemian Massif. Contrib. Mineral. Petrol. 112, 261–278.

O'Brien, P.J., Walte, N., Li, J.H., 2005. The petrology of two distinct granulite types in the Hengshan Mts, China, and tectonic implications. J. Asian Earth Sci. 24, 615–628.

Paquette, J.L., Menot, R.P., Peucat, J.J., 1989. REE, Sm–Nd and U–Pb zircon study of eclogites from the Alpine External Massifs (Western Alps): evidence for crustal contamination. Earth Planet. Sci. Lett. 96, 181–198.

Pearce, J.A., 1982. Trace element characteristics of lavas from destructive plate boundaries. In: Thorpe, R.S. (Ed.), Andesites: Orogenic Andesites and Related Rocks. John Wiley and Sons, Chichester, pp. 525–547.

Pearce, J.A., Norry, M.J., 1979. Petrogenetic implications of Ti, Zr, Y and Nb variations in volcanic rocks. Contrib. Mineral. Petrol. 69, 33–47.

Qian, H.W., Li, L.B., Gao, L., Qiu, S.P., 1996. The ductile searing belts of high-pressure granulites and garnet amphibolite in North China platform. Acta Geosci. Sin. 17, 19–29 (in Chinese).

Ravna, E.K., 2000a. The garnet–clinopyroxene Fe^{2+}–Mg geothermometer: an updated calibration. J. Metamorph. Geol. 18, 211–219.

Ravna, E.K., 2000b. Distribution of Fe^{2+} and Mg between coexisting garnet and hornblende in synthetic and natural systems: an empirical calibration of the garnet–hornblende Fe–Mg geothermometer. Lithos 53, 265–277.

Rickwood, P.C., 1968. On recasting analyses of garnet into end-member molecules. Contrib. Mineral. Petrol. 18, 175–198.

Shervaris, J.W., 1982. Ti–V plots and the petrogenesis of modern and ophiolitic lavas. Earth Planet. Sci. Lett. 59, 101–118.

Smelov, A.P., Beryozkin, V.I., 1993. Retrograded eclogites in the Olekma granite-greenstone region, Aldan Shield, Siberia. Precambrian Res. 62, 419–430.

Song, B., Zhang, Y.H., Wan, Y.S., Jian, P., 2002. Preparing of zircon target for SHRIMP analysis, age measurements and discuss about the observations. Geol. Rev. 48, 26–30 (Supp., in Chinese).

Spear, F.S., Markussen, J.C., 1997. Mineral zoning, P–T–X–M phase relations and metamorphic evolution of some Adirondack granulite, New York. J. Petrol. 38, 757–783.

Sun, S.S., McDonough, W.F., 1989. Chemical and isotopic systematics of oceanic basalts: implications for mantle composition and processes. In: Saunders, A.D., Norry, M.J. (Eds.), Magmatism in the Ocean Basins, Geol. Soc. Spec. Pub., vol. 42, pp. 313–354.

Vidal, P., Hunziker, J.C., 1985. Systematics and problems in isotope work on eclogites. Chem. Geol. 52, 129–141.

Vincenzo, G.D., Palmeri, R., 2001. An ^{40}Ar–^{39}Ar investigation of high-pressure metamorphism and the retrogressive history of mafic eclogites from the Lanterman Range (Antarctica): evidence against a simple temperature control on argon transport on amphibole. Contrib. Mineral. Petrol. 141, 15–35.

Williams, I.S., 1998. U–Th–Pb geochronology by ion microprobe. In: McKibben, M.A., Shanks III, W.C., Ridley, W.I. (Eds.), Applications of Microanalytical Techniwues to Understanding Mineralizing Processes, Rev. Econ. Geol., vol. 7, pp. 1–35.

Winchester, J.A., Floyd, P.A., 1977. Geochemical discrimination of different magma series and their differentiation producta using immobile elements. Chem. Geol. 20, 325–343.

Yang, T.N., 2001. Early retrometamorphism of the Donghai eclogite: the formation and characteristics of symplectite and its geological implications. Acta Geol. Sin. 75, 91–96 (in Chinese).

Zhai, M.G., 1996. Granulites and Lower Continental Crust in North China Archaean Craton. Seismological Press, Beijing, pp. 1–239.

Zhai, M.G., Guo, J.H., Li, J.H., Li, Y.G., Yan, Y.H., Zhang, W., 1996. Retrograded eclogites in the Archaean North China Craton and their geological implication. Chin. Sci. Bull. 41, 315–320.

Zhai, M.G., Bian, A.G., Zhao, T.P., 2000. The amalgamation of the supercontinent of North China Craton at the end of Neo-Archean and its break-up during late Paleoproterozoic and Mesoproterozoic. Sci. China (D) 43, 219–232.

Zhang, Q., Zhou, G.Q., 2001. Ophiolites of China. Sci. Press, Beijing, pp. 44–48 (in Chinese).

Zhao, G.C., 2001. Paleoproterozoic assembly of the North China Craton. Geol. Mag. 138, 87–91.

Zhao, G.C., Wilde, S.A., Cawood, P.A., 1998. Thermal evolution of Archean basement rocks from the eastern part of the North China Craton and its bearing on tectonic setting. Int. Geol. Rev. 40, 706–721.

Zhao, G.C., Wilde, S.A., Cawood, P.A., Lu, L.Z., 1999. Tectonothermal history of the basement rocks in the western zone of the North China Craton and its tectonic implications. Tectonophysics 310, 37–53.

Zhao, G.C., Cawood, P.A., Wilde, S.A., Sun, M., Lu, L.Z., 2000. Metamorphism of basement rocks in the Central Zone of the North China Craton: implications for Paleoproterozoic tectonic evolution. Precambrian Res. 103, 55–88.

Zhao, G.C., Cawood, P.A., Wilde, S.A., Lu, L.Z., 2001. High-pressure granulites (retrograded eclogites) from the Hengshan complex, North China Craton: petrology and tectonic implications. J. Petrol. 42, 1141–1170.